Songklanakarin J. Sci. Technol.
40 (2), 359-366, Mar. - Apr. 2018

http://www.sjst.psu.ac.th

Review Article

Effects of loading rate and temperature on strength and deformability of Maha Sarakham salt

Komkrit Phatthaisong, Suratwadee Sartkaew, and Kittitep Fuenkajorn*

Geomechanics Research Unit, Institute of Engineering, Suranaree University of Technology, Mueang, Nakhon Ratchasima, 30000 Thailand

Received: 30 June 2016; Revised: 2 October 2016; Accepted: 5 January 2017

Abstract

Uniaxial and triaxial compression tests are performed to assess the effects of temperature and loading rate on strength and deformability of Maha Sarakham salt. Specimens are compressed to failure under constant confining pressures between 0 and 12 MPa while the axial stress is increased at constant rates of 0.001, 0.01, and 0.1 MPa/s. Elasticity and strength at dilation and at failure increase with loading rates. Sets of empirical equations are derived for the strength, temperature, and applied stress rate in forms of power, logarithmic, and exponential functions. The distortional strain energy at dilation and at failure varies linearly with the mean normal stress. The proposed strength criteria are applied to determine the safe maximum withdrawal rate of a compressed-air energy storage cavern in the Maha Sarakham formation. The strain energy criterion that considers both distortional and mean stress-strain tends to give the most conservative result.

Keywords: rock salt, strain energy, elasticity, strength, dilation

1. Introduction

Effects of loading rate on the compressive strength and deformability of intact rocks have long been recognized (Cristescu & Hunsche, 1988; Fuenkajorn *et al*., 2012; Kumar, 1968). A primary concern of the rate-dependent effect arises when one applies the laboratory-determined properties of intact rock to stability analysis of rock under in-situ conditions. Strength and elastic properties obtained from laboratory test under a relatively high loading rate, normally about 0.5-1.0 MPa per second (ASTM D7012-07), are usually greater than those of in-situ rocks during excavation or construction. This may lead to a non-conservative design of structures. For rocks exhibiting creep behavior, such as rock salt, the loading rate strongly affects their mechanical responses. The main mechanisms governing the rate-dependent deformability and strength of rock salt involve the dislocation glide, dislocation climb, healing and fracture initiation and propagation (Cristescu & Hunsche, 1988; Fuenkajorn & Daemen, 1988; Fuenkajorn *et al*., 2012). Experimental results obtained by Sriapai *et al*. (2012) indicate that compressive and tensile strengths and elasticity of rock salt decrease with an increase in temperature. The loading rate and thermal effects play a significant role on the stability analysis and design of the pressure schemes for compressed-air, liquefied petroleum gas (LPG), and natural gas storage caverns in salt (Jeremic, 1994). Experimental and theoretical researches have long been performed, notably as part of nuclear waste disposal programs, to truly understand the time-dependent deformation (creep) of salt under elevated temperatures and pressures. Rare attempt, however, has been made to determine the thermal and rate-dependent strengths of the salt, particularly under confined conditions. The strength criterion that can take the loading rate and temperature effects into consideration is also rare.

The objective of this study is to experimentally assess the effects of temperature and loading rate on the compressive strength and deformability of rock salt. Uniaxial and triaxial compression tests have been performed on Maha Sarakham salt using a polyaxial load frame with applied loading rates from 0.001 to 0.1 MPa/s, temperatures from 303 to 473 Kelvin, and confining pressures from 0 to 12 MPa.

*Corresponding author
Email address: kittitep@sut.ac.th

Multi-axial empirical criteria that can take loading rate and temperature effects into consideration are proposed to describe the dilation and failure of the salt. Supported by numerical simulations, these criteria are applied to calculate the safe maximum withdrawal rates of a compressed air energy storage cavern in the Maha Sarakham salt formation under elevated temperatures.

2. Sample Preparation

The tested specimens belong to the Lower Salt member of the Maha Sarakham formation. The formation hosts several solution-mined caverns in the basin. It is also being considered as a host rock for compressed-air energy storage (CAES) caverns by the Thai Department of Energy, and for chemical waste disposal by the Office of Atomic Energy for Peace. The planned CAES cavern is an upright cylinder with 50 m diameter and 300 m height. Top of the cavern (casing shoe) is at 500 m. The cavern has spherical top and bottom. Warren (1999) gives the origin and geological description of the Maha Sarakham salt. The tested salt is virtually pure halite, with a slight amount of clay inclusions (less than 1%). Drilled cores were dry-cut to obtain cubical shaped specimens with nominal dimensions of (58×58×58) mm^3. Over 60 specimens were prepared. The average density is 2.18±0.04 g/cm^3.

3. Test Apparatus and Method

A polyaxial load frame (Fuenkajorn & Kenkhunthod, 2010) has been used to apply constant lateral and axial stresses to cubical salt specimens (Figure 1). The axial load is applied by a 1,000-kN hydraulic load cell connected to an electric oil pump via a pressure regulator. Six steel plates transmit loads to the salt specimens. They can be wrapped with heater coils connected to digital controller and thermostat, which allows testing under elevated temperatures. The heating system can maintain constant temperature to the nearest ±5 Kelvin. After installing the cubical salt specimen into the load frame, dead weights are placed on the two lower bars to obtain the pre-defined the uniform lateral stress (σ_3) on the specimen. Simultaneously the vertical stress is increased to the pre-defined σ_3 value. Neoprene sheets are placed at the interface between loading platens and rock surfaces to minimize the friction. Uniform lateral confining pressures (σ_2=σ_3) on the salt specimens range from 0, 3, 7, to 12 MPa, and the constant vertical stress rates ($\partial\sigma_1/\partial t$) from 0.001, 0.01, to 0.1 MPa/s until failure. The test is started by increasing the vertical stress at the predefined rate using the electric pump. The specimen deformations are monitored in the three loading directions and are used to calculate the principal strains during loading. The readings are recorded every 10 kN (or about 3.43 MPa) of load increment until failure. The failure loads are recorded and the mode of failure is examined. For elevated temperature testing, the prepared specimens and loading platens are pre-heated for 24 hours before testing (Figure 1). A digital temperature regulator is used to maintain constant temperature of the specimen within the range of 5 K.

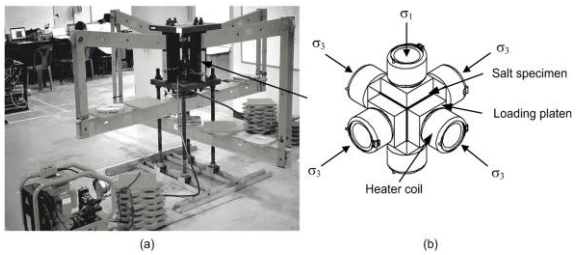

Figure 1. Polyaxial load frame (a) and loading platens wrapped with heater coil (b).

4. Test Results

Figure 2 shows the stress-strain curves of salt specimens tested under 303 and 473 K. The specimens tend to show nonlinear behavior, particularly under high temperatures and low loading rates. Salt compressive strengths increase with loading rates. The thermal effects can be observed by the reduction of the salt strength. This holds true for all loading rates. Strength results obtained under ambient temperature agree well with those determined by Fuenkajorn *et al*. (2012) who conduct triaxial testing on the same salt.

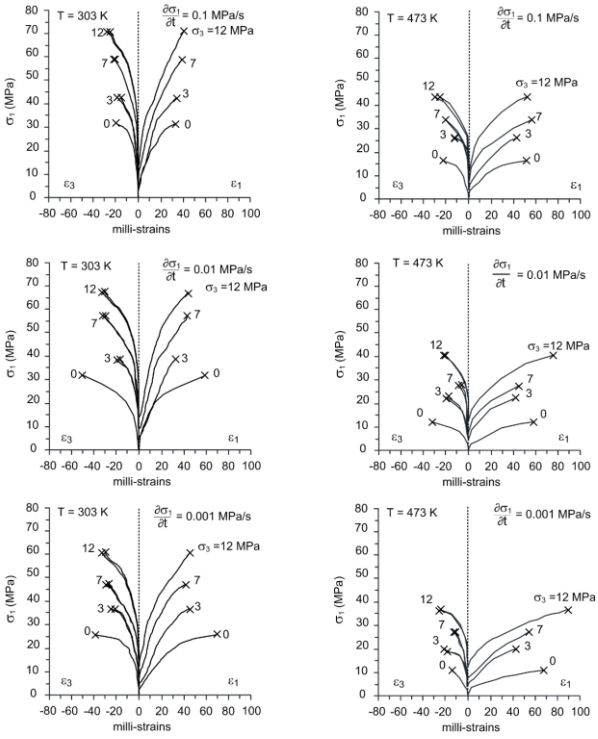

Figure 2. Axial and lateral strains for various confining pressures with testing temperatures at 303 K and 473 K.

Under low temperature and high loading rate the salt fails by extensile splitting. This mode dominates when it is subjected to lower loading rates. Under elevated temperatures the specimens tend to deform plastically and fail by compressive shear mode. The applied octahedral shear stresses (τ_{oct}) are plotted as a function of octahedral shear strain (γ_{oct}) in Figure 3. The τ_{oct} and γ_{oct} can be derived from Jaeger *et al*. (2007):

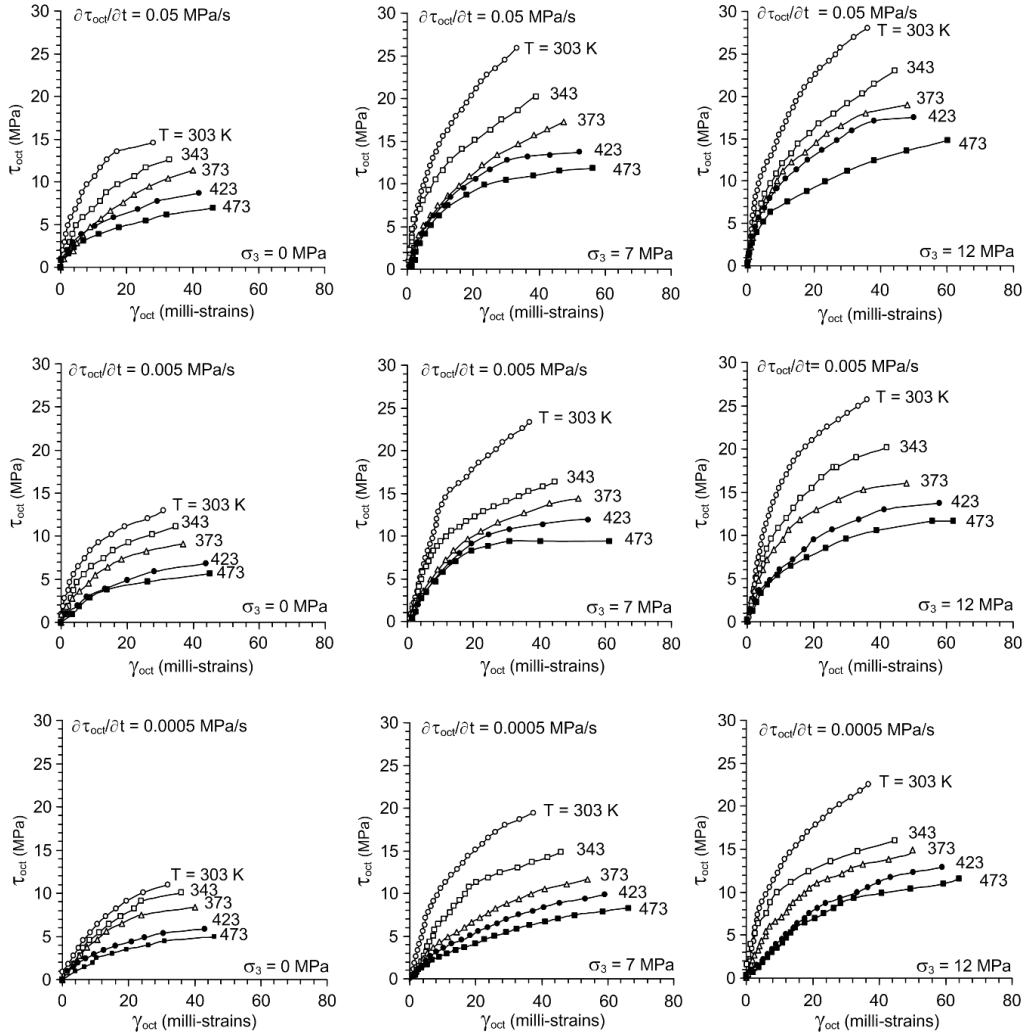

Figure 3. Octahedral shear stresses as a function of octahedral shear strain.

$$\tau_{oct} = (1/3)\left[(\sigma_1-\sigma_2)^2+(\sigma_1-\sigma_3)^2+(\sigma_2-\sigma_3)^2\right]^{1/2} \quad (1)$$

$$\gamma_{oct} = (1/3)\left[(\varepsilon_1-\varepsilon_2)^2+(\varepsilon_1-\varepsilon_3)^2+(\varepsilon_2-\varepsilon_3)^2\right]^{1/2} \quad (2)$$

where ε_1, ε_2 and ε_3 are the major, intermediate and minor principal strains. In this study $\sigma_2 = \sigma_3$. Since σ_2 and σ_3 are constant with time here, the following relation is obtained:

$$\partial\tau_{oct}/\partial t = (\sqrt{2}/3)\partial\sigma_1/\partial t \quad (3)$$

Higher shearing rates applied result in higher shear strengths and lower shear strains at failure. The thermal effect is enhanced when the confining pressures are increased.

5. Elastic Properties of Maha Sarakham Salt

The deformation moduli along the three principal directions can be derived from the elastic stress-strain relations (Jaeger *et al*., 2007):

$$\varepsilon_1 = \sigma_1/E_1 - \nu(\sigma_3/E_{3,N} + \sigma_3/E_{3,E}) \quad (4)$$

$$\varepsilon_{3,N} = \sigma_3/E_{3,N} - \nu(\sigma_1/E_1 + \sigma_3/E_{3,E}) \quad (5)$$

$$\varepsilon_{3,E} = \sigma_3/E_{3,E} - \nu(\sigma_1/E_1 + \sigma_3/E_{3,N}) \quad (6)$$

where $\varepsilon_{3,N}$ and $\varepsilon_{3,E}$ are the mutually perpendicular minor principal strains, E_1 is the deformation modulus along the vertical (σ_1) axis, and $E_{3,N}$ and $E_{3,E}$ are the deformation moduli along the two lateral principal axes. The above equations are used in the calculation to determine whether the deformation moduli along the three principal axes are equal. The results indicate that the Poisson's ratios tend to be independent of the loading rate and temperature. Their values range from 0.37 to 0.48. The deformation moduli are similar for all principal directions (Figure 4). They range from 9 to 24 GPa. This suggests that the tested salt is isotropic. Figure 5 plots the elastic moduli and Poisson's ratios as a function of temperature. Elastic moduli exponentially decrease as the temperatures increase. They also increase logarithmically with loading rate as indicated by the equation in Figure 5(a). This agrees with the experimental results obtained by Sriapai *et al*. (2012) on the same salt. Higher loading rates result in a higher

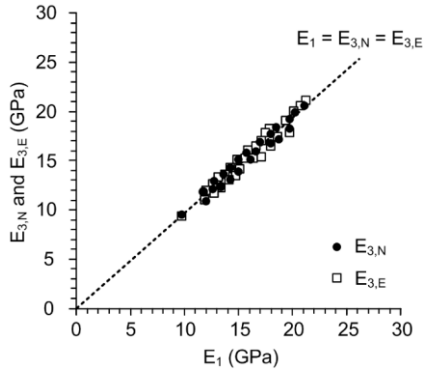

Figure 4. Elastic moduli calculated along the two minor principal axes ($E_{3,N}$ and $E_{3,E}$) as a function of those along the major principal axis (E_1).

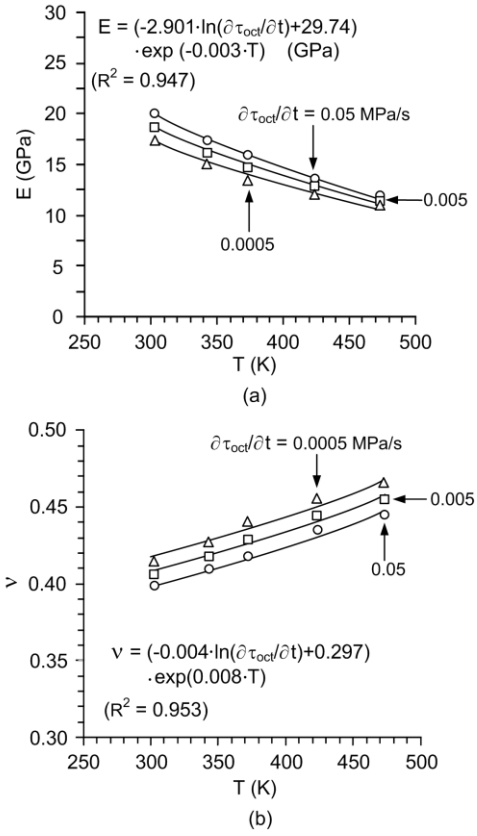

Figure 5. Elastic moduli (a) and Poisson's ratios (b) averaged from the three principal directions and confining pressures as a function of temperature.

elastic modulus of the salt. The Poisson's ratios tend to increase when the temperature increases and the loading rate decreases. This is due to the fact that the salt dilates plastically and more easily when it is subjected to high temperature and slow loading. Under low temperature and quick loading conditions the salt is however more brittle, and hence showing lower dilation. The rate dependency of the salt elastic parameters observed here agrees well with those reported by Fuenkajorn *et al*. (2012) and Sartkaew and Fuenkajorn (2014) who conduct the laboratory testing on rock salt obtained from the Maha Sarakham formation. Fuenkajorn and Daemen (1988) and Jeremic (1994) also conclude that the salt elasticity increases with the applied loading rate. The elastic moduli and Poisson's ratios that are presented as a function of loading rate and temperature given in Figure 5 will later be used in the stability analysis of CAES cavern in the following sections.

6. Octahedral Shear Strength and Shear Stress Rate Relation

An attempt is made to represent the effect of the loading rate under multiaxial conditions. For each specimen the octahedral shear stress at failure ($\tau_{oct,f}$) can be calculated from the principal stresses at failure, as shown in Equation (1). The octahedral shear stress and shear strains at dilation ($\tau_{oct,d}$ and $\gamma_{oct,d}$) can also be calculated from the major principal stresses and the three principal strains at dilation. The dilation stress represents the maximum stress at which the salt remains elastic. The octahedral shear stresses at failure ($\tau_{oct,f}$) and at dilation ($\tau_{oct,d}$) are plotted as a function of the shear rate ($\partial\tau_{oct}/\partial t$) in Figure 6. Interpolation between these σ_m points allows derivation of the $\tau_{oct,f}$ and $\tau_{oct,d}$ as a function of $\partial\tau_{oct}/\partial t$ under the selected magnitudes of σ_m (5, 10, 15, 20 , 25, and 30 MPa), which can be represented by:

$$\tau_{oct,f} = 0.699 \cdot \sigma_m \cdot \dot{\tau}_{oct}^{\,0.075} + 68.05 \cdot \exp(-0.006 \cdot T) \text{ (MPa)} \quad (7)$$

$$\tau_{oct,d} = 0.536 \cdot \sigma_m \cdot \dot{\tau}_{oct}^{\,0.331} + 46.84 \cdot \exp(-0.006 \cdot T) \text{ (MPa)} \quad (8)$$

The empirical constants above are defined by regression analysis using SPSS software (Wendai, 2000). Good correlations are obtained ($R^2 > 0.9$).

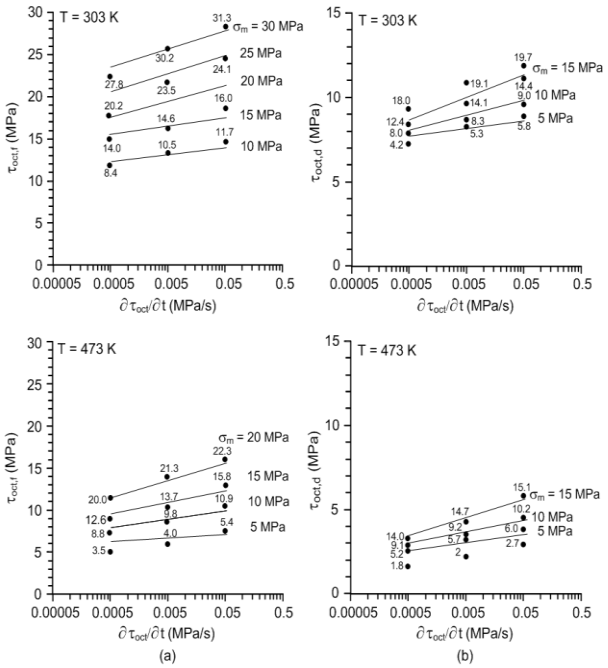

Figure 6. Octahedral shear stresses at failure (a) and at dilation (b) as a function of shear rate for various mean stresses.

7. Octahedral Shear Strength and Shear Strain Relation

The τ_{oct}-$\partial\tau_{oct}/\partial t$ criterion above has been derived without taking the induced strains into consideration. Due to nonlinear behavior of the salt they may not be adequate to predict the rock strength or dilation under very low loading rates and high temperatures. This section proposes shear strength and dilation criterion that takes the corresponding shear strains into account. The octahedral shear stress can be calculated as a function of shear strain, as shown in Figure 7. The empirical equations of these curves can be written as:

$$\tau_{oct,f} = 2.81\times10^{3}\cdot\sigma_m^{\ 0.493}\cdot\gamma_{oct}^{\ 0.037}\cdot T^{-1.105}\cdot(\partial\tau_{oct}/\partial t)^{0.045} \quad \text{(MPa)} \tag{9}$$

$$\tau_{oct,d} = 2.76\times10^{3}\cdot\sigma_m^{\ 0.170}\cdot\gamma_{oct}^{\ -0.018}\cdot T^{-1.818}\cdot(\partial\tau_{oct}/\partial t)^{0.068} \quad \text{(MPa)} \tag{10}$$

The empirical constants are obtained from regression analysis of the test data. Equations give correlation coefficients (R^2) greater than 0.9 for both testing temperatures.

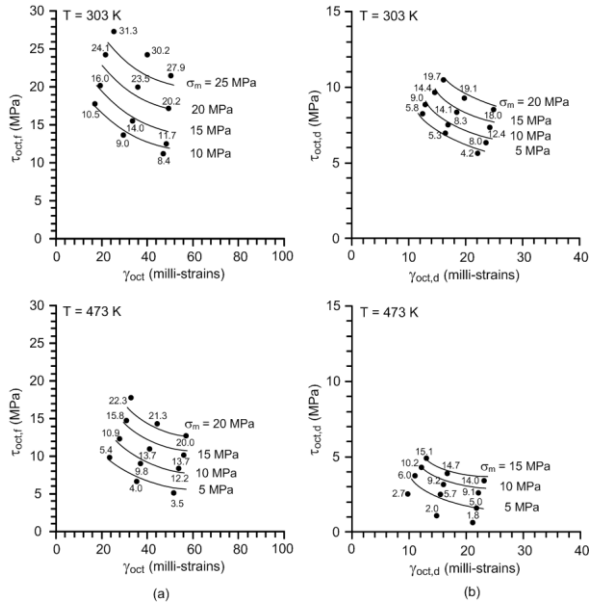

Figure 7. Octahedral shear stresses at failure (a) and at dilation (b) as a function of shear strain.

8. Strain Energy Density Criterion

The strain energy density principle is applied here to describe the salt strength and deformability under different loading rates and temperatures. The distortional strain energy at failure (W_d) and at dilation ($W_{d,d}$) can be calculated from the octahedral shear stresses and strains for each salt specimen using the following relations (Jaeger *et al*., 2007):

$$W_d = (3/2)\cdot\tau_{oct,f}\cdot\gamma_{oct,f} \tag{11}$$

$$W_{d,d} = (3/2)\cdot\tau_{oct,d}\cdot\gamma_{oct,d} \tag{12}$$

The distortional strain energy at failure (W_d) and at dilation ($W_{d,d}$) can also be derived as a function of the mean strain energy density at dilation ($W_{m,d}$), as follows:

$$W_m = (3/2)\cdot\sigma_m\cdot\varepsilon_m \tag{13}$$

$$W_{m,d} = (3/2)\cdot\sigma_{m,d}\cdot\varepsilon_{m,d} \tag{14}$$

$$\sigma_{m,d} = (1/3)\cdot(\sigma_{1,d} + 2\sigma_3) \tag{15}$$

$$\varepsilon_{m,d} = (1/3)\cdot(\varepsilon_{1,d} + \varepsilon_{2,d} + \varepsilon_{3,d}) \tag{16}$$

where $\sigma_{m,d}$ and $\varepsilon_{m,d}$ are the mean stresses and strains at dilation. Figure 8 shows a linear trend of the $W_{d,d}$ –$W_{m,d}$ relation which can be best represented by:

$$W_{d,d} = 1.55W_{m,d} - 0.039 \quad \text{(MPa)} \tag{17}$$

The proposed criterion considers both stress and strain at dilation and hence isolates the effect of stress rate and temperature.

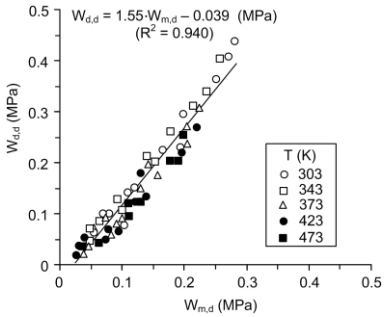

Figure 8. Distortional strain energy at dilation ($W_{d,d}$) as a function of mean strain energy at dilation ($W_{m,d}$).

9. Withdrawal Rate of Compressed-Air Energy Storage Cavern

One operating parameter that dictates the peak energy generation for the compressed-air storage cavern in salt is the air withdrawal rate. The higher withdrawal rate gives the greater peak energy generation. An excessively high rate of pressure reduction, however, could induce dilation or failure of the salt adjacent to and near the cavern boundaries. Determination of the safe withdrawal rate requires a failure criterion that can describe the rate-dependent strength of the salt, such as those proposed in this study.

The finite difference program FLAC (Itasca, 1992) is used here to simulate the single isolated cavern in axial symmetry. The principal stresses and strains induced in the surrounding salt under various air withdrawal rates are calculated and compared against the dilation criteria developed above. The salt cavern and geologic structure are obtained from an exploratory borehole at Nachueak district, Maha Sarakham province. This location is considered as a potential CAES site by Thai Department of Energy. The mesh model represents the cavern from the ground surface to the depth of 1,000 m at Nachueak district. The upright cavern dia-

meter is 50 m, and its height is 300 m. It has a half-spherical roof and bottom.

The in-situ stress is assumed to be hydrostatic. Before cavern development the salt stress at the casing shoe depth (σ_{cs}) is calculated as 10.8 MPa. The maximum cavern pressure is defined as 9.7 MPa (or $0.9\sigma_{cs}$). The preferred minimum pressure is 2.2 MPa ($0.2\sigma_{cs}$). The surrounding salt temperatures are assumed to be uniform at 303 K (30 °C) and 373 K (100 °C). The 100 °C is a conservative estimate as the compressed-air temperature would dissipate into the surrounding salt mass. Each salt temperature is simulated under four different rates of cavern pressure withdrawal: 15.0, 7.5, 0.5 and 0.25 MPa/day (equivalent to pressure schemes of 1 cycle/day, 15 cycles/month, 1 cycle/month, and 6 cycles/ year, respectively). The equivalent pressure schemes are calculated by assuming that the air injection and retrieval periods are equal.

The Maha Sarakham salt is assumed to behave as a Burgers material. The Burgers model is used here to describe the creep deformation and stress distribution of the salt around CAES cavern during retrieval period. Findley *et al*. (1989) and Jaeger *et al*. (2007) provide a governing equation for the Burgers model as:

$$\gamma_{oct} = \tau_{oct}\left[\left(\frac{t}{\eta_1}+\frac{1}{E_1}+\frac{\eta_1}{\eta_2 E_2}\right)-\left(\frac{\eta_1}{\eta_2 E_2}\exp\left(\frac{-E_2 t}{\eta_2}\right)\right)\right] \quad (18)$$

where τ_{oct} is octahedral shear stresses (MPa), t is time (day), E_1 is elastic modulus (GPa), E_2 is spring constant in visco-elastic phase (GPa), η_1 is visco-plastic coefficient in steady-state phase (GPa.day) and η_2 is visco-elastic coefficient in transient phase (GPa.day). These parameters can be calibrated from creep testing where the applied differential stresses are constant. The Burgers parameters for the Maha Sarakham salt are obtained from the calibration results of Samsri (2010) and Archeeploha (2015) who perform creep testing of the same salt under 303 K and 373 K, respectively. These parameters are given in Table 1.

Table 1. Creep properties of Lower Salt member used in FLAC simulations (Samsri, 2010; Archeeploha, 2015).

Parameter	T (K)	
	303	373
Elastic modulus, E_1 (GPa)	1.29	1.19
Spring constant in visco-elastic phase, E_2 (GPa)	3.59	3.37
Visco-plastic coefficient in steady-state phase, η_1 (GPa.day)	86.27	72.75
Visco-elastic coefficient in transient phase, η_2 (GPa.day)	0.71	1.31
Density, γ (g/cm^3)	2.20	2.20

Table 2 summarizes the mean stresses and strains, octahedral shear stresses and strains, and distortional and mean strain energy at the roof of the cavern. They are calculated at 24 hrs after starting withdrawal. The changes of the stress and strains obtained from the computer simulations under withdrawal period are compared with the strength criteria developed in the previous sections. The stability of the cavern roof is of interest in this analysis because during withdrawal it will be subjected to the largest difference between the internal air pressure and the salt in-situ stress. For all cases the mean and shear stresses and strains decrease with the withdrawal rate. The octahedral shear stresses and strains under high temperature at 373 K are greater than those under 303 K.

For a conservative design the surrounding salt is not allowed to dilate during the withdrawal period. As a result the three dilation criteria developed above are used here to calculate the factor of safety (FS) of the salt at the roof of the cavern where it is subjected to the greatest shear stresses. These include τ_{oct}–$\partial\tau_{oct}/\partial t$ criterion (Equation 8), $\tau_{oct,d}$–$\gamma_{oct,d}$ criterion (Equation 10) and $W_{d,d}$–$W_{m,d}$ criterion (Equation 17).

Table 2. Stresses, strains and strain energy density from simulation.

T (K)	Pressure scheme	Pressure withdrawal rate (MPa/day)	σ_m (MPa)	ε_m (10^{-3})	τ_{oct} (MPa)	γ_{oct} (10^{-3})	W_d (MPa)	W_m (MPa)
303	1 cycle/day	8.64	11.59	8.05	2.02	89.43	0.27	0.14
	15 cycles/month	4.32	11.42	7.02	1.91	49.19	0.14	0.12
	1 cycle/month	0.28	10.39	6.34	2.12	20.79	0.07	0.10
	6 cycles/year	0.14	9.63	5.94	2.18	14.43	0.05	0.09
373	1 cycle/day	8.64	12.28	8.45	2.63	95.76	0.38	0.16
	15 cycles/month	4.32	12.05	7.81	2.35	59.62	0.21	0.14
	1 cycle/month	0.28	11.83	6.79	2.03	30.50	0.09	0.12
	6 cycles/year	0.14	10.19	5.69	2.36	15.22	0.05	0.09

The results of FS calculation for all pressure schemes are shown in Figure 9. The FS values obtained under salt temperature of 373 K are lower than those under 303 K. The $\tau_{oct,d}$–$\partial\tau_{oct}/\partial t$ criterion tends to give the largest FS values for all cases. This criterion does not consider the mean stresses and strains induced around the cavern. The $W_{d,d}$–$W_{m,d}$ criterion gives the most conservative results. It shows the FS values lower than 1.0 for the withdrawal rates of 8.64 and 4.32 MPa/day (1 cycle/day and 15 cycles/month). This criterion is perhaps the most appropriate for use in the design of the withdrawal rate because it incorporates both shear and mean stresses and strains. The FS values obtained from applying the $\tau_{oct,d}$–$\gamma_{oct,d}$ criterion are between those obtained from the other two criteria. This criterion does not consider the mean stresses and strains induced around the cavern.

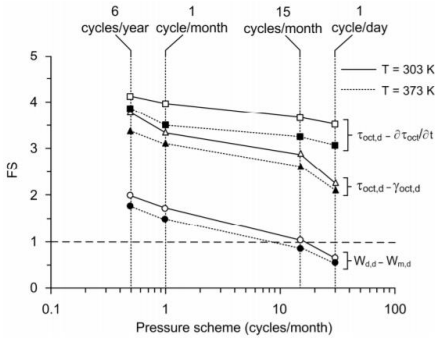

Figure 9. Factors of safety at cavern roof based on the proposed criteria.

10. Discussion and Conclusions

It is recognized that the specimen size used here is relatively small (58×58×58 mm^3). Experimental results obtained by Senseny (1984) indicate that small specimens tend to give greater transient deformation than do the larger ones. The steady-state creep rate of salt, however, tends to be independent of the specimen size (Mirza, 1984). This means that the time-dependent deformation obtained under high loading rate (0.05 MPa/s) in this study may overestimate those induced in salt around the storage cavern during depressurization. This is because the dislocation glide is the main mechanism governing the deformation in the transient creep phase. Under low loading rate testing however the dislocation climb mechanism is predominant which governs the steady-state creep deformation, and hence the visco-plastic parameter calibrated from the test results can adequately describe the time-dependent deformation of salt around storage cavern, particularly under low withdrawal rate.

The salt strengths increase with loading rates which agree with the results obtained elsewhere (Fuenkajorn *et al*., 2012). The decreases of the compressive strengths with increasing temperatures also agree with the experimental results obtained by Sriapai *et al*. (2012). The salt elastic moduli measured at 40% failure stress vary from 9 to 24 GPa, and the Poisson's ratio from 0.37 to 0.48. Higher loading rates result in a higher elastic modulus of the salt. The Poisson's ratios tend to increase when the temperature increases and the loading rate decreases. Both, salt strength and stiffness increase with the loading rate and decrease with the temperature as experimentally evidenced by the increase of the failure stresses and elastic modulus. The decrease of the salt strength as the temperature increases suggests that the applied thermal energy before the mechanical testing makes the salt weaker, and more plastic, causing it to fail at lower stress and higher strain with lower elastic moduli.

The designed safe maximum withdrawal rate depends not only on the site specific conditions, but on the creep laws that are used to describe the time-dependent deformation of the surrounding salt. The Burgers model has been used in the FLAC simulation because it is one of the simple models that can describe the instantaneous response, transient and steady-state creep of the salt. To assess the stability of a salt cavern other more complicated constitutive laws can also be used in determining the stresses and strains around the cavern, and comparing them with the criteria above. Depending on the safety requirements the salt strength criterion at failure may be used instead of the dilation criterion as used here. This will result in a greater FS value for each simulated case.

Acknowledgements

This study was funded by Suranaree University of Technology and by the Higher Education Promotion and National Research University of Thailand. Permission to publish this paper is gratefully acknowledged.

References

Archeeploha, S. (2015). *Effects of thermal and mechanical cyclic loads on time dependent behavior of rock salt* (Master's thesis, Suranaree University of Technology, Nakhon Ratchasima, Thailand).

ASTM International. (2007). *Compressive strength and elastic moduli of intact rock core specimens under varying states of stress and temperatures. ASTM D7012.* West Conshohocken, PA: Author.

Cristescu, N. D., & Hunsche, U. (1988). *Time effects in rock mechanics.* Hoboken, NJ: John Wiley and Sons.

Findley, W. N., Lai, S. J., & Onaran, K. (1989). *Creep and relaxation of nonlinear viscoelastic materials: with an introduction to linear viscoelasticity*. New York: NY: Courier Dover.

Fuenkajorn, K., & Daemen, J. J. K. (1988). *Borehole closure in salt, Technical report prepared for the U.S. Nuclear Regulatory Commission* (Report No. NU REG/CR-5243 RW). Tucson, AZ: University of Arizona.

Fuenkajorn, K., & Kenkhunthod, N. (2010). Influence of loading rate on deformability and compressive strength of three Thai sandstones. *Geotechnical and Geological Engineering, 28*, 707-715.

Fuenkajorn, K., Sriapai, T., & Samsri, P. (2012). Effects of loading rate on strength and deformability of Maha Sarakham salt. *Engineering Geology, 135-136*, 10-23.

Itasca Consulting Group. (1992). *User manual for FLAC-Fast langrangian analysis of continua* (Version 4.0). Minneapolis, MN: Author.

Jaeger, J. C., Cook, N. G. W., & Zimmerman, R. W. (2007). *Fundamentals of rock mechanics* (4th ed.). Milton, Australia: Blackwell Publishing.

Jeremic, M. L. (1994). *Rock mechanics in salt mining*. Rotterdam, The Netherlands: A.A. Balkema.

Kumar, A. (1968). The effect of stress rate and temperature on the strength of basalt and granite. *Geophysics, 33*(3), 501-510.

Sartkaew, S., & Fuenkajorn, K. (2014). Effects of loading rate on strength and deformability of rock salt under 273-373 kelvin. *Proceedings of the ISRM International Symposium – 8th Asian Rock Mechanics Symposium.* Sapporo, Japan.

Senseny, P. E. (1984). Specimen size and history effects on creep of salt. *Proceedings of the First Conference on the Mechanical Behavior of Salt*, *Federal Republic of Germany*, 369-379.

Mirza, U. A. (1984). Prediction of creep deformations in rock salt pillars. *Proceedings of the first conference on the mechanical behavior of salt*, *Federal Republic of Germany*, 311-337.

Samsri, P. (2010). *Determination of creep properties of rock salt using modified point load testing* (Master's thesis, Suranaree University of Technology, Nakhon Ratchasima, Thailand).

Sriapai, T., Walsri, C., & Fuenkajorn, K. (2012). Effects of temperature on compressive and tensile strengths of salt. *Science Asia, 38*, 166-174.

Warren, J. (1999). *Evaporites: Their evolution and economics*. Oxford, England: Blackwell Science.

Wendai, L. (2000). *Regression analysis, linear regression and probit regression. In 13 chapters, SPSS for windows: Statistical analysis*. Beijing, China: Publishing House of Electronic Industry.